Influence of shaft stiffness on the performance of a plane-like hydrofoil

Agathe de la Hougue, Guillaume Androuin, Laetitia Pernod, Matthieu Sacher, Benoît Augier, Patrick Bot, Paul Iachkine

Influence of shaft stiffness on the performance of a plane-like hydrofoil

A. DE LA HOUGUE [abc], G. ANDROUIN [a], L. PERNOD [b], M. SACHER[c], B. AUGIER [a], P. BOT [b], Paul IACHKINE [d]

a. IFREMER, benoit.augier@ifremer.fr
b. IRENav Ecole Navale, patrick.bot@ecole-navale.fr
c. ENSTA Bretagne, CNRS UMR 6027, IRDL, matthieu.sacher@ensta-bretagne.fr
d. ENVSN, paul.iachkine@envsn.sports.gouv.fr

Keywords: Hydrofoils, Velocity Prediction Program, Free Surface Interaction, FSI

Abstract:

Hydrofoils are now widely used to reduce hydrodynamic resistance, leading to increased velocities and sailing crafts performance. However, designing hydrofoils for sailing vessels such as windfoils and kitefoils remains a complex challenge, as the ride height plays a critical part on the stability and performance of foiling vessels. Furthermore, the strut between the board and the plane-like foil (called the shaft) is highly loaded and subject to significant deformation, leading to potentially important Fluid-Structure Interaction (FSI) effects. Consequently, it is now critical to consider the ride height and the FSI effects in Velocity Prediction Programs (VPP). This work first presents the development of a novel five degree-of-freedom (DoF) Velocity Prediction Program (VPP) for foiling crafts, which includes the FSI effects on the shaft of the vessel. Hydrodynamic forces are computed using a vortex lattice model with a viscous correction, solved by the panel method implemented in the software Athena Vortex Lattice (AVL). The structural behavior of the shaft is introduced in the VPP in the form of an analytical model derived from experimental tests on real shafts. This improved VPP is then applied to a generic plane-like hydrofoil, typical of a windfoil sailing upwind at a speed of 9m/s (18kts) and approximately a 20° windward-heel. Twenty shafts of different stiffness are tested, and their respective deflections, as well as the equilibrium state computed by the VPP, are compared. Results show that for a static analysis the equilibrium state and the performance are barely affected by the stiffness of the shaft. However, the use of a flexible shaft leads to a different distribution of the lateral hydrodynamic force (anti-drift) onto the different parts of the foil.

.

1 Introduction

Hydrofoils are used to partially or fully support a ship's weight, thus reducing the hydrodynamic resistance as a significant fraction of the ship's hull is lifted out of the water. The use of lifting hydrofoils as a means of drag reduction consequently caused a jump in yacht performance and increased velocities over the recent years. However, as flying crafts are relatively new, these series have not yet reached the same level of expertise as older yacht racing series. In particular, designing hydrofoils for sailing races such as the America's Cup or the Olympics remains a complex challenge since the hydrofoil has to achieve boat flying conditions as much as possible, while i) minimizing drag over a large range of boat speeds and while ii) keeping the craft as stable and manoeuvrable as possible. For small foiling crafts, T-foils or plane-like hydrofoils are now widely used, as they offer a good trade-off between the generated lift, the total drag and the equilibrium of the submersed system. These foils are characterized by a horizontal lifting surface connected to the craft by a vertical shaft. The performance can be studied

thanks to Velocity Prediction Programs (VPP) where the equilibrium of the foiling craft is solved for different sailing conditions. VPPs have been developed for different sailing vessels, from classical high-performance boats [Philpott et al. 1993] to foiling catamarans [Bagué et al, 2021, Graf et al. 2020], including dinghies such as lasers [Day 2017]., with an increased complexity in the physical phenomena considered and the numerical methods used. For instance, [Day 2017] takes into account the sail power and the position of the crew, and [Bagué et al, 2021, Graf et al. 2020] use numerical methods from lifting line to full CFD. The influence of the structure deformation may also be considered thanks to the introduction of FSI effects in the VPP, such as in the case of foiling 60ft Imoca [Horel and Durand 2019] or L foils on catamarans [Graf et al. 2016].

An important parameter in the dynamics of foiling crafts that needs to be considered in Velocity Prediction Programs (VPP) is the height of flight (Hagemeister and Flay 2019), as it plays a critical role on the side force and the drag through the wetted area. Indeed, the ride height is often one of the key factors in the foiling equilibrium and stability. The issue of the optimum height of flight for the sail craft "moth" equipped with T-Foils is studied both experimentally [Kebbell et al., Binns et al.] and numerically with the evaluation of a lifting line method [Day 2017].

This work focuses on the behaviour of windfoils (foiling winfsurfs) which are equipped with a plane-like foil package composed of a shaft, a main wing and a smaller rear wing called stabilizer, connected by a fuselage (Figure 1). When foiling, the craft flies around 0.7m above the water surface with a speed from 15 up to 30 knots (7.5 up to 15 m/s) and with great fluctuations in attitudes (for example during a "stable" flight, the heel angle may vary by up to 10°). Important issues on the windfoil are thus the effect of the free surface and the deformation of the shaft, as this slender structure is heavily loaded. The interaction with the free surface is indeed an important characteristic of the windfoil with a surface piercing shaft and horizontal lifting surfaces being at low depth or sometime surface piercing. The performance of hydrofoils close to a free surface has been presented in the literature both experimentally and numerically for a single extruded NACA foil [Ni et al. 2021, Daskovsky 2000] or in tandem configuration [Bal 2007] with a diminution of the lift and increase of the drag when getting closer to the surface.

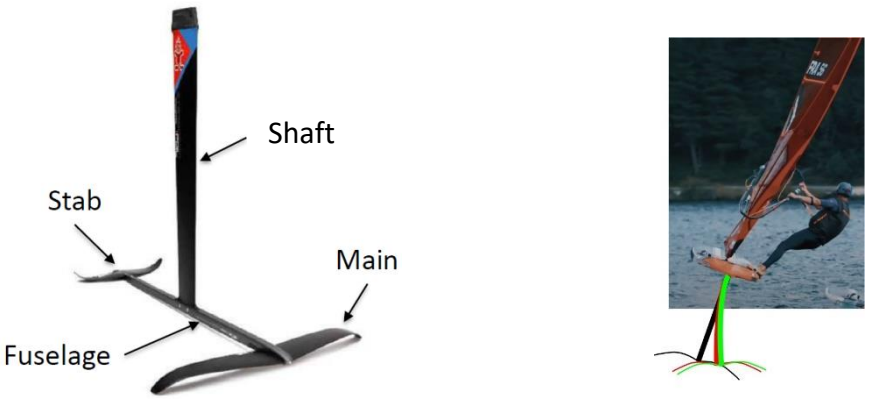

Figure 1: Olympic windfoil plane-like hydrofoil and structure displacement under loading (artist's view)

Performance predictions of foiling sailing crafts have motivated numerous studies, with a particular interest recently on the issue of stability (see for example Graf et al. 2016, Kerdraon et al. 2020, Bagué et al. 2021). Velocity Prediction Programs are also used to optimize foil and sail trimming [Day 2017,

Graf et al. 2020]. Binns et al. [2008] measured the forces produced by a Moth T-foil rudder and found no change of efficiency when the heel angle is increased from 0° to 30°. They gave results on the variations of lift and drag with the depth-to-chord ratio. Day et al. [2019] performed tank testing on monohull dinghy T-foils and showed that a lifting line approach was correct for low angles of attack. They tested two different submergence heights and found a reduced drag close to the surface. Daskovsky [2000] found a decrease in lift when the foil gets closer to the free surface for moderate angles of attack. Ni et al. (2021) showed the same trend with a sharp decrease for submergence-to-depth ratio lower than one. The fluid structure interaction (FSI) of foils has been studied by numerous authors. For example, Temtching Temou et al [2021] investigated the hydro-elastic response of a composite hydrofoil with models of different levels of fidelity and highlighted the importance of the bend-twist coupling (see also Pernod et al. [2019]). However, FSI is rarely considered by the commonly used VPPs. As a notable exception, Horel and Durand (2019) studied a foiling Open60 monohull and found that the foil flexibility had little influence on the lift and drag, but significantly affects the side force and changes how the loading is distributed among the different appendages.

This work investigates the effect of the deflection of the shaft on the performance of a generic plane-like hydrofoil typical of a windfoil using of 5 Degrees of Freedom (DOF) Velocity Prediction Program (VPP: resolving the balance between aero and hydrodynamic forces to find the operating point). The hydrofoils are heavily loaded and thus deformed depending on the stiffness of the shaft and the height of flight. A simplified structural model is proposed thanks to experimental test on shaft to represent the Fluid Structure behaviour of the foil subjected to hydrodynamic loading. Results obtained with a rigid shaft are compared with results obtained with flexible shafts of different stiffness values.

2 Velocity Prediction Program (VPP)

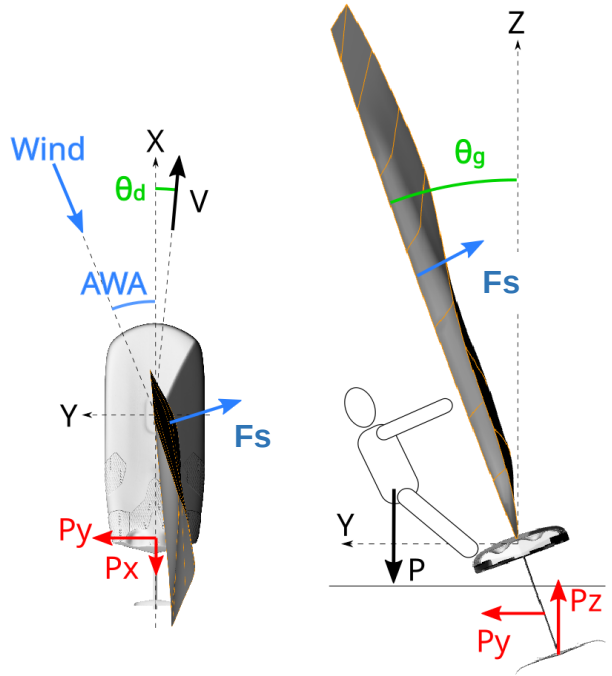

Figure 2: Forces on the windfoil. AWA is the Apparent Wind Angle, P is the total weight (sailor+ equipment), Fs is the aerodynamic force from the sail, Px, Py, Pz are the three components of the total hydrodynamic force Ff from the foil package (shaft+main wing+stabilizer).

This study focuses on the performance prediction of a foiling windsurf, namely a windfoil. The sailing craft is composed of a 9m² sail, a 2.2m long board and a plane-like hydrofoil. The hydrofoil, presented on Figure 1, is composed of a plane based on a main wing (0.095m²) and a stabilizer (0.025m²) connected by a fuselage. The plane is connected to the board by the help of a vertical shaft, itself a 1m long free-surface piercing composite structure with a symmetric section.

In the present work, it is considered an upwind sailing point of a rigid body formed by the sail, the board and the athlete (see Figure 2), while the shaft of the foil is the only structure allowed to deform.
As shown in Figure 2, the craft is sailing at an apparent wind angle AWA which is obtained from a vector construction of the true wind and the speed V of the craft. The craft is sailing with a heel angle Θg to windward (opposite to common non-foiling yachts), a small trim angle Θa which mainly affects the angle of attack of the foil (main wing and stabilizer), and finally a small drift angle Θd is also considered, which is commonly called the leeway angle, that mainly affects the angle of attack of the submerged portion of the shaft. In order to study the influence of different tuning parameters on the performances of the windfoil, a 5 degree-of-freedom (DOF) VPP has been implemented to solve:

1. Speed V
2. Leeway angle Θd
3. Heel angle Θg
4. Height of flight Tz
5. Trim angle Θa

The yaw balance is the only unsolved degree of freedom. To ease the VPP convergence, some parameters remain also fixed. Indeed, the opening angle of the sail (around Z-axis when Θg=Θa=0°) is set to 13.5° while its trim angle (around Y-axis when Θg=Θa=0°) is set to -10°. It should be noted that since a rigid body (sail, board and athlete) is considered, the craft angles Θd, Θg and Θa also affect the forces and moments of the sail. The sailor position from the reference point in Figure 2 is also set to -0.4m, 1.4m and 1m for respectively X, Y and Z axis when Θg=Θa=0°.
The considered nonlinear system of forces and moments equations to be solved is given by,

$$\sum \vec{F} = \overrightarrow{F_f} + \overrightarrow{F_s} + \vec{P} = \vec{0} \qquad (1)$$

$$\sum \vec{M} = \overrightarrow{M_f} + \overrightarrow{M_s} + \overrightarrow{M_P} = \vec{0} \qquad (2)$$

where, $\overrightarrow{F_s}$ is the aerodynamic force from the sail and $\overrightarrow{F_f}$ is the hydrodynamic force of the foil. The weight of the athlete and the craft $\vec{P}$ is also considered. In equation (2), moments are computed at the reference point (i.e. bottom of the sail mast). The aerodynamic loads of the board and the athlete are not considered. The system of equations (1) and (2) is solved using the Newton-Raphson method and the convergence of the VPP is reached when the residual of both forces and moments are below a convergence threshold fixed to 1N and 1N.m.

3 Numerical force models

In the present section, numerical models to compute aerodynamic and hydrodynamic loads that are used in the VPP are presented.

3.1 Aerodynamic loads

In order to model the aerodynamics of the sail, sail shape measurements have been carried out by the ESPCI – Paris. More precisely, the sail has been hoisted on its mast without wind and each sail batten has been measured with 10 points to then reconstruct the whole sail surface. In the present work, this

sail shape is used in the VPP and FSI on the sail and mast are neglected. Aerodynamic loads on the sail are determined with a Vortex Lattice Method (VLM). The following hypotheses are considered: inviscid fluid, incompressible and irrotational flow, profile thickness is neglected and turbulence is not modelled. The surface of the sail is discretized into several quadrilateral panels, each one composed of an unknown horseshoe vortex and a control point to prescribe that the normal velocity across the panel is zero. The numerical solution of the lifting surface problem computes each vortex strength then to determine the forces and moments generated by the fluid on the studied thin body. The VortexLattice Julia-based code of Taylor McDonnell and Andrew Ning [Day, 2017] is presently used to compute the sail aerodynamic loads. VortexLattice has been designed and validated [Day, 2017] to obtain fast and consistent results for stationary and unsteady flows.

A VLM mesh convergence analysis has been carried out and has led to discretize the sail with 1250 elements: 50 along the span and 25 along the chord, as shown on Figure 3. The discretization along the span is refined near the top and bottom, using a cosine distribution, to better model the circulation drop.

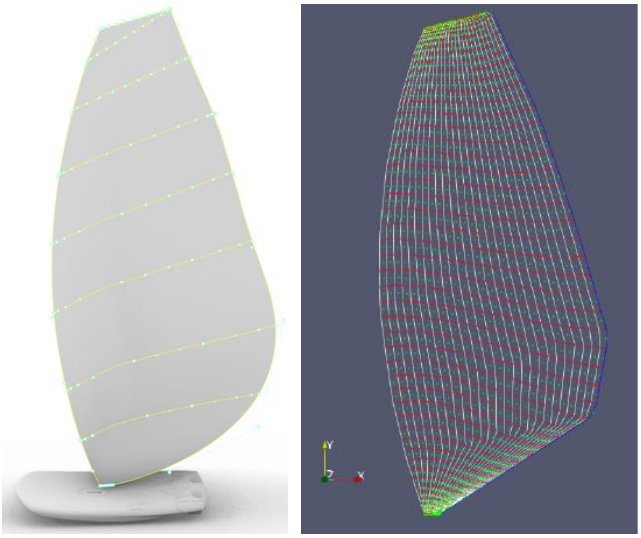

Figure 3: Points measured on the real sail (left) and meshed sail (right)

3.2 Hydrodynamic loads

The geometry of the foil (i.e. profile, chord and span) has been built from an average of commercially available windfoil geometries. Hydrodynamic loads on the three lifting surfaces of the foil (shaft, main wing and stabilizer) are computed with the Athena Vortex Lattice (AVL) code [Drela and Youngren 2011], also based on the VLM. A viscous correction is added to account for the viscous drag, which is estimated with the XFOIL code [Drela, 1989], based on a 2D panel method where a coupled viscous-inviscid interaction approach is employed. The free surface effects can be modelled in a simplified way but at a low computation cost by using a symmetry or an anti-symmetry condition on the free surface plane. It is generally admitted that the symmetry condition is more adapted to low-Froude number situations [Temtching Temou et al. 2021] while the anti-symmetry condition is more suitable for high Froude numbers [Faltinsen 2005, Dutton 2017] (see also Perali et al. 2022). In the present work, the foil chord-based Froude number is of order 10 which leads to the anti-symmetry condition as free surface model. This anti-symmetric plane is set at the position corresponding to the flying height and the part of the shaft above the free surface is not considered.

Figure 4 shows the influence of the free surface on the hydrodynamic forces of the foil. Total forces of the foil (main, shaft and stabilizer) are reported and given along X (drag), Y (lateral force) and Z (upward force) components. Forces are scaled by hydrodynamic forces at infinite submergence and are plotted as functions of h/c, where h is the shaft submergence and c is the shaft chord length. Specifically, when h=1m, the shaft is fully submerged whereas when h=0m, the shaft is completely out of the water. Results observed in Figure 4 are in line with what is expected [Binns et al. 2008, Pernod et al. 2022]. The drag (X) and the lateral (Y) forces decrease as the foil is getting closer to the free surface which can be explained by the reduction of the wetted surface of the shaft. The lift force (Z) firstly increases as the foil gets closer to the free surface because of the acceleration of the flow between the horizontal wing and the free surface. When the foil gets too close to the free surface (h/c below ≈ 1), the lift brutally drops.

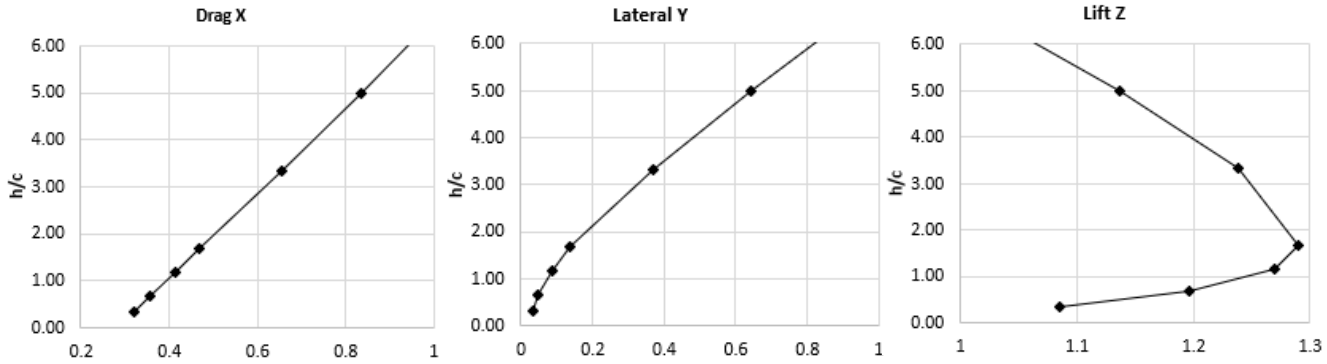

Figure 4: h/c versus hydrodynamic forces on the foil scaled by forces at infinite submergence

The free surface effects, as functions of the flying height, on hydrodynamic forces seem to be correctly predicted and this model can thus be used in the VPP to account for effects of the craft flying height on hydrodynamic forces of the foil. For instance, the VPP should be able to model the compromise between flying higher to reduce drag, and keeping enough submersion to achieve the necessary vertical lift and side force.

3.3 Fluid Structure Interaction on the shaft

While sailing, the hydrofoil is subjected to a lateral force, which is mainly distributed on the immersed part of the shaft. Thus, the shaft is deformed which, in the end, might influence the lift created and the way of sailing. In this section, a model to determine the deformation of the shaft while sailing is proposed. This model is based on bending tests and the beam theory.

Punctual load

First, a shaft is tested as a cantilevered beam subjected to a point load on its free end. This type of load is easier to apply than a distributed load and is suitable to determine the mechanical characteristics. As the analytical expression is known from beam theory [Fanchon 2019], the identification of stiffness properties is possible (Eq 3).

$$v_{ponctual}(x) = \frac{-Fx^2}{6\,EI}\,(3L - x) \qquad (3)$$

where $v_{ponctual}(x)$ is the deflection of the beam at the section x, F is the force, L is the total length of the beam, E is the Young's modulus and I is the quadratic moment.

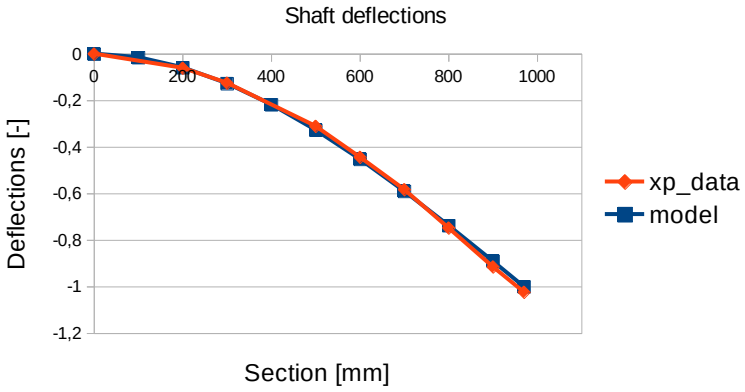

Figure 5: Deflection of the shaft for a point load; model compared to tests

This form assumes that E and I are constant along the beam, which in our case is not rigorously exact. However, if the deflection calculated with this model is fitted to the experimental values measured, the average EI product can be identified as can be seen on Figure 5. It appears that the deflection shape is rather well represented with a maximum deviation of 5,11% at 500mm. In this study, the nonlinear effects are neglected and the EI calculated with the experiment is supposed to stay the same whatever the value of the force applied. For this study, a punctual load of 20kg is applied on the shaft at x=900mm. The deflection at this point is measured experimentally and the EI corresponding to the shaft is calculated thanks to equation (3). Twenty shafts were tested and a range of values for EI are found.

Distributed load

While sailing, the load is not punctual but distributed on the immersed part. Here, the load is considered uniform between the water surface and the end of the shaft. Using beam theory, the deflection shape can be calculated (Eq. 4).

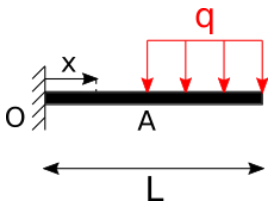

Figure 1: Application of a distributed load between section A and L

$$0 \le x \le A \;\; v_{OA}(x) = q\frac{A-L}{EI}\left[\frac{L+A}{4}x^2 - \frac{1}{6}x^3\right]$$
$$A \le x \le L \;\; v_{AL}(x) = \frac{q}{24\,EI}\left[-(L-A)^4 + 4x(A^3 - L^3) + L^4 - A^4\right] \qquad (4)$$

where :

- A is the first section immersed
- L is the total length of the shaft
- q is the distributed load, also defined using the first model as q = F/(L-A)
- E is the Young's modulus
- I is the quadratic moment of the section.

The deflection of the whole shaft is then computed using equation (4) with the EI previously identified from the tests and considering a distributed load *q=F/(L-A)* with F the lateral force on the shaft and L-A=Tz, the immerged part of the shaft depending on the height of flight.

4 Results

4.1 Deflection of the shaft for different stiffness

The VPP is run to find the operating point of sail at equilibrium for different values of the shaft stiffness. The stiffness range investigated is larger than what is measured on actual foils, in order to highlight the effects of deformation and test if optimum values may exist even out of the existing range. VPP runs are done for the following cases:

- Perfectly rigid shaft, called "No deformation"
- The highest EI value measured, called "stiff"
- The lowest EI value measured, called "flexible"
- Intermediary EI value equal to 85% of maximum, called 85%
- More flexible shafts with EI equal to 75% and 50% of maximum, called 75% and 50%.

Figure 7 represents the deflection of the shaft when the VPP has reached the equilibrium in each of these cases. The deflection in mm is shown as a function of the z coordinate along the shaft (1000 mm is the top of the shaft where the board is and 0 mm is the bottom, where the fuselage is).
As expected, the more flexible the shaft, the higher the deflection at the end. For a shaft with EI 50% lower than the stiffest shaft tested, the deflection at the bottom of the shaft is almost twice as high. It should be noted that this most flexible case is close to the limit of validity of the linear deformation theory used here.

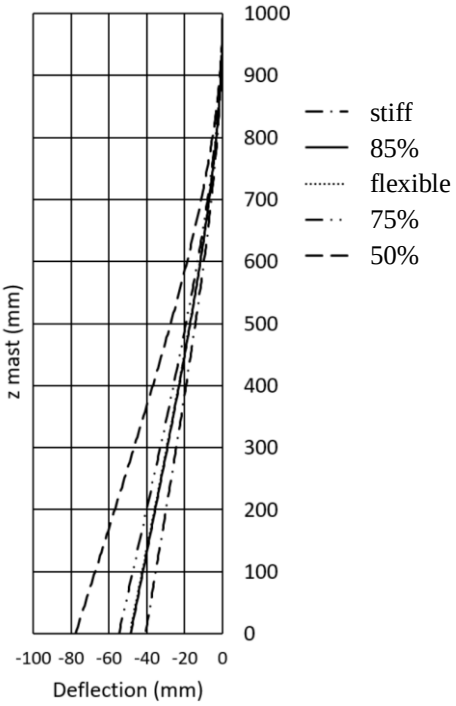

Figure 7: Shaft deflection at equilibrium for the different considered stiffness of the shaft for the upwind sailing condition

4.2 Converged values of the parameters of the VPP

In the following graphs presented in Figure 8, the converged values of the different parameters of the VPP are plotted for the different EI simulated. These values are compared to results obtained for the shaft with no deformation. It can be observed that a difference exists between a non-elastic shaft and the others where the balance point is not the same. In addition, the trend of the evolution of the balance values is consistent with the deformation of the shaft. The leeway angle $|\theta_d|$ and the heel angle $|\theta_g|$ grow as the flexibility increases whereas the height of flight (L-Tz) and the craft velocity decrease. However, in the range of stiffness measured on actual foils, the variation in balance point between the most flexible and the stiffest foils is very low. Figure 9 illustrates the equilibrium point reached for a perfectly rigid shaft and the most flexible investigated case – EI=50% – with a shaft half as stiff as the stiffest measured. In this study, where only a static equilibrium is computed and the stability is not considered, the effect of the stiffness is thus not that important. However, as illustrated in Fig.9, the stiffness of the shaft does affect the projections of forces and the contribution of the main wing and stab to the lateral force along the Y axis.

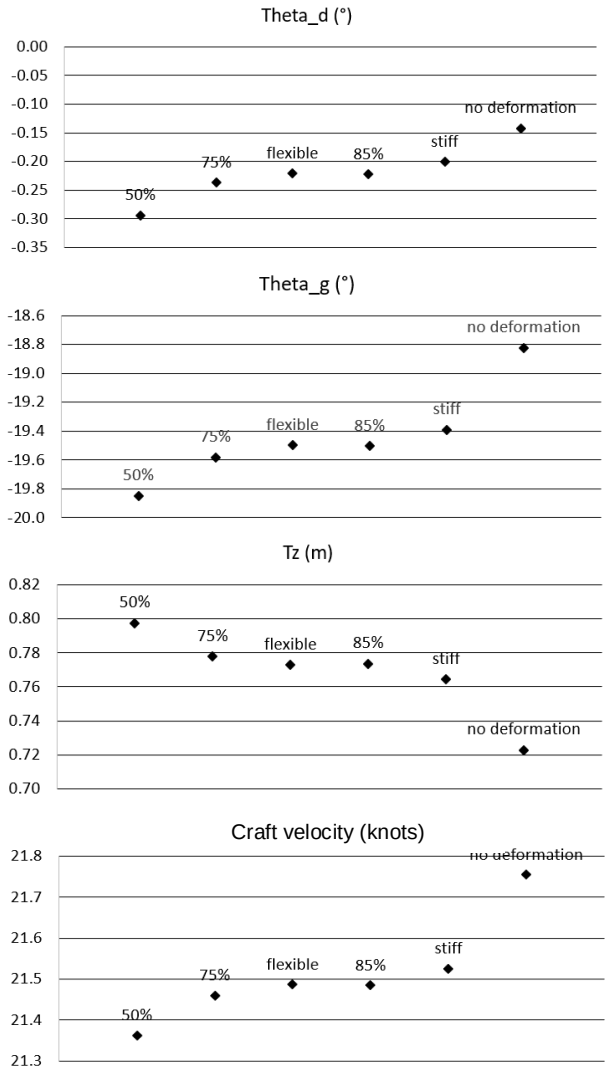

Figure 8: Effect of shaft stiffness on the angles, height of flight and speed of the windfoil

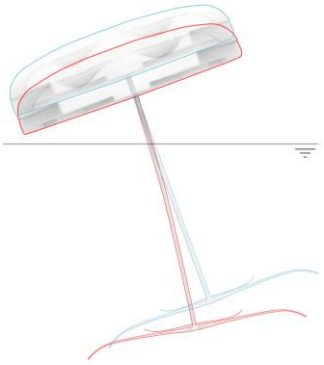

Figure 9: Effect of shaft stiffness on the angles and height of flight: Blue is a reference case with a perfectly rigid shaft and Red is 50% stiffness shaft

4.3 Distribution of the lateral force

Even if the point of equilibrium and the performance are barely affected by the deformation of the foil, it is noticeable that the lateral hydrodynamic force (anti-drift) which is necessarily produced to balance the aerodynamic side force is distributed differently among the different parts of the foil, when the shaft is deformed. Figure 10 shows the distribution of lateral force for the different considered stiffness of the shaft. On this graph (Fig. 10), the total anti-drift force (Py_tot) is plotted as well as the contribution from each part: the main wing, the stabilizer (negative contribution) and the shaft, for different values of shaft stiffness. What can be observed is that as the shaft is more flexible, the lateral force from the main wing is decreasing as the wing is more horizontal, and the contribution of the shaft to the side force increases. This is also correlated to the increase of the leeway angle which results in a higher angle of attack for the shaft. For a perfectly rigid shaft, most of the anti-drift force is given by the main wing thanks to the windward heel, which allows the craft to foil higher, meaning low submerged area of the shaft. For the most flexible shaft studied (50%), the contributions of the shaft and the main wing to the side force are similar, compensated by a lower height of flight.

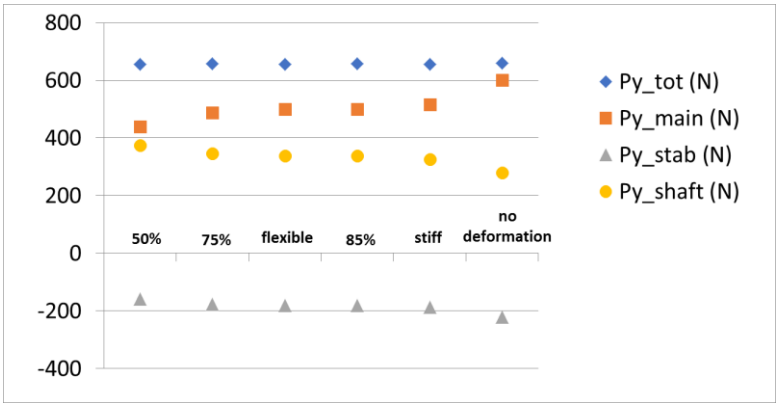

Figure 10: Effect of shaft stiffness on the side force Py distribution between the different lifting surfaces of the hydrofoil

4 Conclusions

This paper presents the development of a novel five degree-of-freedom (DoF) VPP for foiling crafts, which includes the FSI effects on the shaft of the vessel. Hydrodynamic forces are computed using a

vortex lattice model with a viscous correction, solved by the panel method implemented in the software Athena Vortex Lattice (AVL). The structural behavior of the shaft is introduced in the VPP in the form of an analytical model derived from experimental tests performed on twenty shafts. Shafts of different stiffness are tested, and their respective deflections, as well as the equilibrium state computed by the VPP, are compared.
Results show that, even if the deflection varies with the stiffness of the shaft, for a static analysis the equilibrium state and the performance are barely affected. However, the use of a flexible shaft leads to a different distribution of the lateral hydrodynamic force (anti-drift) on the different parts of the foil. The stiffer the shaft, the more the anti-drift force is created by the main wing allowing the craft to fly higher.
Further work is underway in two directions. First, in the model for the deformation of the foil, only the lateral force on the shaft was considered and its effect to deflect the shaft. In reality, the horizontal foil can also be deformed and the shaft is submitted to an horizontal compressive force. In addition, during this study, the sailor was kept in a fixed position. It would be interesting to see if, by changing the position of the center of gravity of the sailor, a more elastic shaft could be interesting in terms of performance compared to a stiffer shaft.Last but not least, only the upwind sailing condition is simulated. The downwind situation, with a typical speed around 15m/s (30kts) and heel angle around 5° could also be investigated.

Acknowledgments

This work was supported by Region Bretagne and the Agence Nationale de La Recherche (ANR) through grant n°ANR-19-STHP-0002. The authors are grateful to the technical staff at IFREMER and ENVSN for their help in the experiments, ESPCI for the sail shape and the FFV for the contribution in the shaft characterization study.

References

1. Bagué, A., Degroote, J., Demeester, T., Lataire, E., 2021, *Dynamic stability analysis of a hydrofoiling sailing boat using CFD*. Journal of Sailing Technology, 6(01): p. 58-72.
2. Bal, S. 2007. "*High-speed submerged and surface-piercing cavitating hydrofoils, including tandem case*". Ocean Engineering 34 (14-15):1935-46.
3. Binns, J.R., P.A. Brandner, and J. Plouhinec, 2008 *The effect of heel angle and free-surface proximity on the performance and strut wake of a moth sailing dinghy rudder t-foil*. in The 3rd High Performance Yacht Design Conference, Auckland
4. Daskovsky, M., 2000, "*The hydrofoil in surface proximity*," Ocean Engineering 27, pp. pp. 1129-1159
5. Day, A. H. 2017. *Performance prediction for sailing dinghies*. Ocean Engineering, 136, 67-79.
6. Day, S., M. Cocard, and M. Troll 2019, *Experimental measurement and simplified prediction of T-foil performance for monohull dinghies*, in The 23rd Chesapeake Sailing Yacht Symposium. 2019: Annapolis, USA
7. Drela, M., 1989. Xfoil: *An analysis and design system for low Reynolds number airfoils*. Springer Berlin Heidelb. 54, 112.
8. Drela M. and Youngren H., "*Athena Vortex Lattice (AVL),"* Ver. 3.32, http://web.mit.edu/drela/Public/web/avl/, Massachusetts Inst. of Technology, Cambridge, MA, 2011
9. Dutton T. S., 2017, *An Investigation into the Design of Surface Piercing Super Cavitating Hydrofoils*, MSc thesis, Massachusetts Institute of Technology
10. Faltinsen, O. M., 2005, *Hydrodynamics of High-Speed Marine Vehicles*, Cambridge University Press
11. Fanchon, J.L., 2019, *Guide de la mécanique*, chapter 26, Nathan
12. Graf, K., Renzsch, H. & Meyer, J., 2016. *Prediction and Optimization of Aerodynamic and Hydrodynamic Forces and Boat Speed of Foiling Catamarans with a Wing Sail and a Jib*. in the 22nd Chesapeake Sailing Yacht Symposium. Annapolis, Maryland, USA

13. Graf, K., Freiheit, O., Schlockermann, P., & Mense, J. C. 2020. *VPP-driven sail and foil trim optimization for the Olympic Nacra 17 foiling catamaran*. Journal of Sailing Technology, 5(01), 61-81
14. Hagemeister, N. and Flay, R. 2019, *Velocity prediction of wing-sailed hydrofoiling catamarans*. J Sailing Technol 4 (01):66-83
15. Horel, B., et Durand, M. 2019. *Application of system-based modelling and simplified-fsi to a foiling open 60 monohull*. Journal of Sailing Technology, 4(01), 114-141
16. Kebbell, S. and Binns, J. 2021. *Development of a Full Scale Moth Hydrofoil Control System Test Rig*. In The 9th Conference on Computational Methods in Marine Engineering (Marine 2021)
17. Kerdraon, P., Horel, B., Bot, P., Letourneur, A., & Le Touzé, D. 2020. *Development of a 6-DOF Dynamic Velocity Prediction Program for offshore racing yachts*. Ocean Engineering, 212
18. McDonnell, T. et Ning, *A. VortexLattice.jl*. url : https://flow.byu.edu/ VortexLattice.jl/dev/#. (visited 07.02.2022).
19. Ni, Z., Manhar, D., and Tsung, C.S. 2021. "*Performance of a Hydrofoil Operating Close to a Free Surface over a Range of Angles of Attack*." International Journal of Naval Architecture and Ocean Engineering 13: 1–11
20. Perali, P., Sacher, M., Lerous, J.B., Wackers, J., Augier, B., Hauville, F., Bot, P., 2022, *Comparaison de conditions de surface libre linéarisées pour l'étude d'un Hydrofoil submerge à l'aide d'une approche potentielle*, 25ème Congrès Français de Mécanique, Nantes
21. Pernod, L., Ducoin, A., Le Sourne, H., Astolfi, J.-A., Casari, P., 2019, *Experimental and Numerical Investigation of the Fluid-Strucure Interaction on a Flexible Composite Hydrofoil under Viscous Flows*, Ocean Engineering, vol. 194, (106647)
22. Pernod, L., Sacher, M., Wackers, J., Augier, B., Bot, P., 2022, *Free-Surface Effects on Two-Dimensional Hydrofoils by RANS-VOF* Simulations, 23rd Chesapeake Sailing Yacht Symposium, SNAME, Annapolis, USA
23. Philpott, A. B., Sullivan, R. M., & Jackson, P. S. 1993. *Yacht velocity prediction using mathematical programming*. European Journal of Operational Research, 67(1), 13-24
24. Temtching Temou, V., Augier, B., and Paillard, B. 2021. *Hydro-elastic response of composite hydrofoil with FSI*. Ocean Engineering, 221.